Behavioural Study of High Carbon Steel Material in Hot and Cold Working Media: A Review

Imhade P. Okokpujie [1,2], *Efetome S.* Odudu[1], *Tamitayo M.* Azeez[1], *Anthony O.* Onokwai[3], *Frederick O.* Ahmadu[4], *Adeyinka O.M.* Adeoye[1]

[1]Department of Mechanical and Mechatronics Engineering, Afe Babalola University, Ado Ekiti, 360001, Nigeria
[2]Department of Mechanical and Industrial Engineering Technology, University of Johannesburg, Johannesburg, 2028, South Africa
[3]Mechanical Engineering Department, Bells University of Technology, Ota, Ogun State, Nigeria
[4]Department of Sociology, Afe Babalola University, Ado-Ekiti, Ekiti State, Nigeria

Abstract: Due to its exceptional mechanical properties, such as its high strength and hardness, high-carbon steel is utilised extensively in various industries. The way of behaving of high-carbon steel is impacted by various handling strategies, for example, hot working and cold working, which can influence its microstructure and mechanical properties. The review aims to Study the behaviour of high-carbon steel material in hot and cold working media. Also, to look at the effects of hot and cold working on the macrostructure of the high carbon steel and the mechanical properties such as hardness, comprehension, impact tests, tensile stress and strain analysis. From the review, the hot and cold working processes, such as bending, rolling, and squeezing, for the result obtained from the hardness test shows the hardness value for hot rolling is higher than that of cold rolling (it is generally expected for hardness obtained from cold rolling should be higher than that from hot rolling) this may be due to the variations in the rolling parameters. While the hardness obtained from cold bending s higher than that from hot bending, and the hardness value obtained from hot squeezing is higher than that of cold squeezing. The results for hot bending of high-carbon steel show improved ductility and reduced risk of cracking compared to cold bending. This viable finding is highly significant to manufacturers to enable the production of sustainable materials for structural applications.

Keywords: High Carbon Steel, Hot and Cold Working Media, Annealing and Normalizing method, Heat treatment

1. Introduction

A high amount of carbon, usually between 0.6% and 1.5% by weight, is present in high-carbon steel, a particular form of steel. Due to its exceptional tensile strength, wear resistance,

and longevity, it is one of the strongest and hardest steel forms. High-carbon steel is frequently used in products like wire, springs, blades, and cutting tools. However, since it is more fragile than lower carbon steels, it needs to be handled with greater care and heat treated to prevent breaking or cracking. The precise carbon content of high-carbon steel might change based on the alloy and production method. Due to its excellent strength and durability, high-carbon steel is utilised extensively in various industrial applications [1]. However, high carbon steel's heat treatment procedure may impact its mechanical qualities. Determining how various heat treatment procedures, such as annealing, quenching, and tempering, impact the mechanical characteristics of high-carbon steel is the research challenge.

The advanced knowledge of the connection between high carbon steel's heat treatment and mechanical properties offers useful advice for enhancing the heat treatment procedure to enhance high carbon steel's performance in industrial applications. The elevated temperature softens the steel, making it more malleable and easier to bend without fracture. The results of cold bending of high-carbon steel depend on factors such as the specific steel grade and its composition. High-carbon steel typically exhibits lower ductility than low-carbon steel, posing challenges and risks of cracking or fracture during cold bending. The values obtained from the review show that the Impact value obtained after hot rolling is higher than that of cold rolling (It is generally expected that hardness obtained from cold, the Impact value of cold bending is higher than that of hot bending, and the Impact value of cold squeezing if higher than hot squeezing. For SEM analysis, cold working produces strain hardening and changes the grain structure, resulting in higher strength but perhaps decreased ductility and toughness. In contrast, hot working refines the microstructure and enhances the mechanical characteristics of high-carbon steel. In conclusion, studying the effect of hot and cold working on high-carbon steel reveals important insights into the material's microstructural changes and mechanical properties. Hot working improves formability, toughness, and ductility, while cold working increases strength and hardness but reduces ductility and toughness. To optimise the performance of high-carbon steel, further research should focus on characterising microstructural changes, optimising mechanical properties, exploring post-processing techniques, investigating fracture and fatigue behaviour, and assessing the industrial application [2].

This study investigates how high-carbon steel's mechanical and metallurgical characteristics are affected by hot and cold working. This research will contribute to understanding how hot and cold working affect high carbon steel's microstructure and mechanical characteristics. The research on the impact of hot and cold working on high-carbon steel will be the main subject of the literature study. The microstructure, mechanical characteristics, and techniques for hot and cold working of high-carbon steel will all be covered. High carbon steel specimens will be acquired, hot- and cold-worked, and then analysed. The specimens will be heated above the recrystallisation temperature during the hot working process and then rolled or forged into the appropriate shape.

2. Behavioral Study of High Carbon Steel Material in Hot working media

According to Drozd et al. [3], the tribological performance of metalworking steel tools is crucial in cold and hot working operations. Coatings are one method for extending the life of metal tools. This study compares five reference tool steels—X155CrVMo12-1, X37CrMoV5-1, X40CrMoV5-1, 40CrMnMo7, and 90MnCrV8—as well as AlCrSiN-coated and bare steel K340 to determine how they wear out quantitatively and by what wear processes. The tool steels under investigation underwent heat treatment, whereas K340 underwent thermochemical processing before being coated with an AlCrSiN thick film

(K340/AlCrSiN). We examined the hardness, chemical makeup, phase structure, and microstructure of K340 and K340/AlCrSiN steels. By ASTM G99, tribological tests were performed using the ball-on-disc tester. An Al 2 O 3 ball was the counter body for the experiments conducted under dry, unidirectional sliding circumstances. The wear factor and coefficient of friction were determined and examined regarding the hardness and alloying content of the materials under investigation. To determine the sliding wear processes of the examined tool steels and PVD-coated K340 steel, scanning electron microscopy (SEM) examinations were undertaken. With AlCrSiN, abrasive wear predominates as opposed to the severe abrasive-adhesive wear mechanism for uncoated tool steels. Figure 1 shows how the investigated materials' friction coefficient varies with distance. The thin coating that was formed successfully shields the K340 substrates from severe wear and deterioration. The K340/AlCrSiN sample also has a coefficient of friction (COF) of 0.529 and a wear factor of K = 5.68 10 7 m 3 N 1 m 1, compared to the reference tool steels' COFs of 0.70 to 0.89 and wear factors of 1.68 10 5 to 3.67 10 5 m 3 N 1 m 1 for the same materials. The AlCrSiN deposition enhances the sliding characteristics and decreases the wear of K340 steel, making it a viable technique for extending the useful life of metalworking tools.

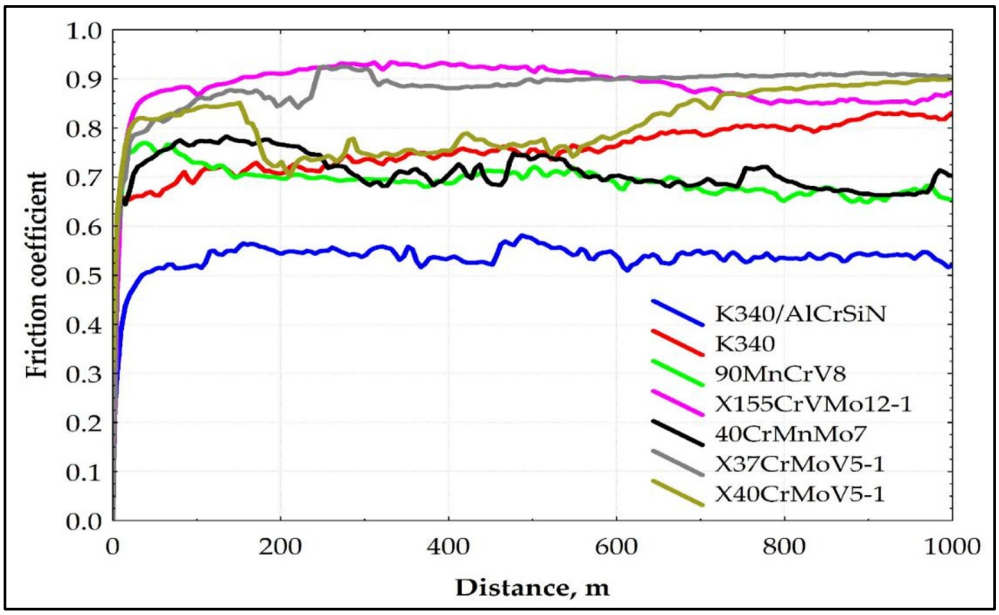

Figure 1: Curves showing how the investigated materials' friction coefficient varies with distance. [3]

The recently created medium-entropy alloy (MEA) has sparked significant interest because of its promising mechanical characteristics. Many alloys' grains are often refined using plastic deformation techniques, such as hot working, to increase their strength, hardness, and wear resistance at low temperatures [4]. The grain refining process under the deformation process on MEA, particularly for CrCoNi, has recently been documented in a few findings. In this study, plastic deformation under various circumstances was purposefully chosen to reveal the fundamental grain refinement process in CrCoNi MEA alloy. The surprising appearance of continuous dynamic recrystallisation during hot deformation of CrCoNi alloy, in contrast to many other alloys with low stacking fault energy, is demonstrated as the primary mechanism for grain refinement of the present alloy.

Furthermore, the work of Murugesan et al. [5]. Designing and optimising the process parameters in the industrial practice of metal forming requires a consistent and realistic

characterisation of the material behaviour under the combined effects of strain, strain rate, and temperature on the material flow stress. This work aimed to develop an adequate flow stress model to characterise the flow behaviour of AISI-1045 medium carbon steel throughout a useful range of deformation temperatures (650-950 °C) and strain rates (0.05-1.0 s1). The Johnson-Cook flow stress model was subsequently used for simulating and forecasting material flow behaviour at high temperatures. Also, surrogate models based on the constitutive relations were created, and the model constants were determined using the results of the experiments. This led to the creation of the constitutive flow stress model, which was then thoroughly tested against experimental data using numerical and graphical validations. Figure 2 Hot tensile tests conducted at various temperatures and strain rates yielded genuine strain-true stress data. Additionally, the Johnson and Cook failure model was applied to predict the behaviour of the material damaged, and seven different specimens, including flat, smooth round bars and pre-notched specimens, were tested at room temperature under quasi-strain rate conditions to establish the model's parameters. The results show that the created model overpredicts the material's behaviour at low temperatures for all strain rates. Nevertheless, the created model can generate a rather precise and accurate assessment of flow behaviour under high-temperature settings, with a strong connection to the experimental data.

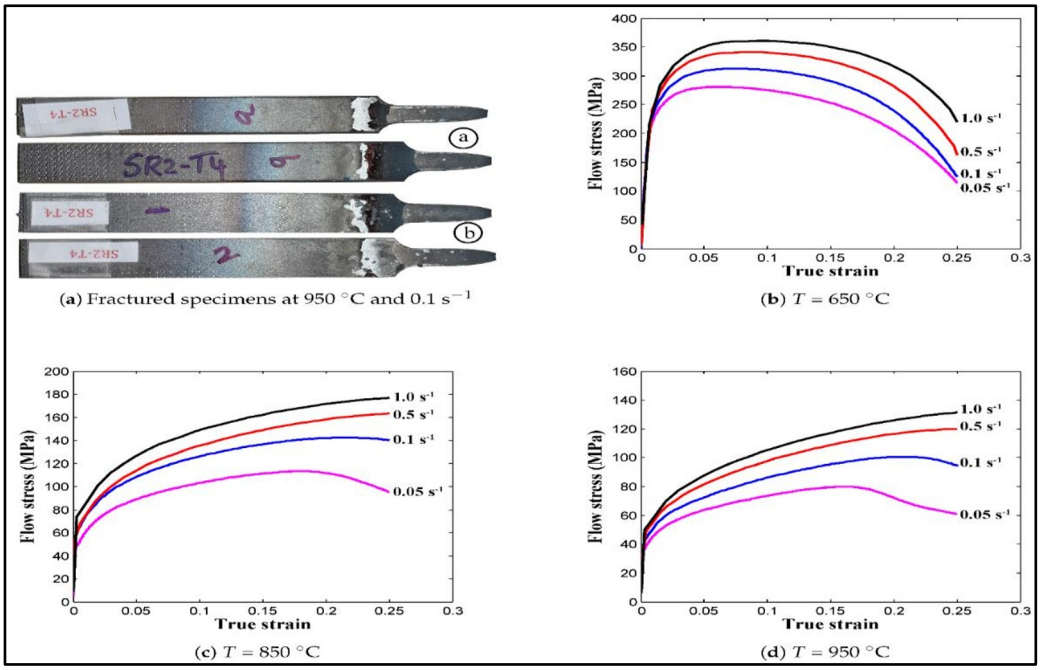

Figure 2: Hot tensile tests conducted at various temperatures and strain rates yielded genuine strain-true stress data. [4]

Holzweissig et al. [6] It was done to characterise the microstructure of hot work tool steel that had undergone selective laser melting. The findings provided insight into how processing parameters and microstructural evolution interact. During layer-wise processing, it was discovered that martensite, which changes to austenite in a later tensile test, makes up a portion of the microstructure. This enhances the hot work tool steel's mechanical characteristics, permitting direct application. Saboori et al. [7]. At 1000–1200 °C and strain rates of 0.001–1 s1, the hot working behaviour of additively produced Ti–6Al–4V pre-forms by electron beam melting (EBM) has been investigated. A wrought Ti-6Al-4V alloy was also

examined for comparison in the same way as the EBM alloy. The data assessments were done step-by-step to explore the hot working behaviour of these samples, and the stepwise process was detailed. Following the hot compression, no localised strain resulting from shear band development was discovered in the samples. Peak stress was visible in the flow stress curves of all the samples at low strains, followed by a regime of flow softening and a nearly constant flow at big strains. Interestingly, the initial microstructure, porosity content, and material chemistry (such as oxygen concentration) may have contributed to the reduced flow stress levels. Interestingly, the initial microstructure, porosity content, and material chemistry (such as oxygen concentration) may all have contributed to the reduced flow stress, which is advantageous from an industrial standpoint. Based on the microstructure of the specimens before and after the heat deformation, the flow softening mechanism(s) was(were) thoroughly examined. The little fluctuation in the flow-softening curves of the EBM samples' appearance might potentially be explained by dynamic recrystallisation (DRX).

Kumar et al. [8] The impact of Al concentration on high-Mn, low-density alloys' hot deformation behaviour Solitary bond single bond Mn at 850–1050 °C and strain rates of 0.001–10 s1, a 3D processing map was used to analyse single bond steels. Compared to the low-Al steel (394 kJ/mol), the high-Al steel had higher flow stress and activation energy (443 kJ/mol). The deformation parameters affect the microstructures of 8Al steel and 10Al steel. For both steel sheets, the recrystallised structure and substructures have displaced the original hot rolling microstructure, while the unstable zone contains deformation bands and flow localisation. The DRX process is significantly inhibited when the Z content rises with rising Al concentration, creating an unstable domain with deformation zones and flow localisation. With a drop-in strain rate to 0.001s1, the shape and distribution of ferrite for high-Al steel change from continuous band ferrite to discontinuous granular ferrite, and the flow localisation characteristics are also not visible. Also, when the Al concentration grows, the fraction of each strain's instability area increases, which reduces the Fesingle bond's capacity to function. Single bond Mn steels with only one bond. Mohammad et al. [9] Studying the constituent behaviour of the recently created Mg-Gd alloys allowed researchers to determine how adding Gd affected how magnesium deformed at high temperatures. It was discovered that 0.5 weight percent Gd is insufficient to raise the flow stress level. In contrast, when 1.5 weight percent of Gd was added, enough Gd atoms were in the solution to cause a considerable rise in flow stress. Based on a thorough constitutive analysis and with the help of creep theories, it was discovered that the glide and climb of dislocations in the climb-controlled regime oversaw the hot deformation of pure magnesium. In contrast, the glide-controlled regime (viscous glide) was responsible for the deformation of the Mg-1.5Gd alloy. Ming-Song et al. [10] Investigations were made on the dynamic recrystallisation (DRX) behaviour of the magnesium alloy AZ31B with a high starting grain size. The DRX kinetics model was created using two different techniques. One is based on DRX volume fraction values assessed using real stress-strain curves (Model 1). The second is based on DRX volume fraction values assessed using optical micrographs (Model 2). It is discovered that Model 1's anticipated DRX volume % is much higher than Model 2's. It shows that the real stress-strain curves for the magnesium alloy AZ31B with a large initial grain size cannot be used to derive the value of DRX volume fraction (Xdrx). Analysis and discussion of the cause were conducted to comprehend the phenomena. We discovered that the primary cause is the magnesium alloy AZ31B's strong fine-grain strengthening (FGS) effect. Two factors will have the most impact on the flow behaviour for the material under study during DRX: 1) The decline in average dislocation density, which causes the flow stress to decline, and 2) The decline in average grain size, which causes the flow stress to rise. The latter results in a greater DRX volume percentage than the genuine one as measured by the true stress-strain curves.

The study's findings will be useful guides for assessing the DRX volume percentage of other FGS materials with high initial particle sizes.

According to Rajeshwar et al. [11] An equiatomic high entropy refractory HfNbTaTiZr alloy with a BCC structure was studied for its hot-deformation behaviour. BCC single phase was compressed uniaxially at temperatures between 1000 and 1200 °C and strain rates between 104 and 102 s1, all stable. Stress-strain graphs showed evident abrupt dips upon yielding and continued reductions in flow stress afterwards. Interrupted compression studies revealed that the sudden reduction in stress might be attributed to dislocation unlocking, either by the atmosphere of the solute atom(s) or short-range ordering. Flow stress analysis was performed using a power law connection of the Arrhenius type. According to data on flow stress, the apparent activation energy (Q) for hot deformation ranged from 258 to 232 kJ mol1 across the whole strain range. The research revealed that flow stress has a high strain rate sensitivity (m) of (m 0.33). A potential of grain boundary sliding (GBS) in the fine-grained DRX regions was suggested by the comparatively high m value and dynamically recrystallised (DRX) microstructures made up of coarse un-recrystallized areas and fine DRX grains with necklace morphologies. The HfNbTaTiZr alloy's slow diffusion may cause limited grain development following DRX, as evidenced by the fine DRX grain sizes. In the un recrystallised coarse portions, preferred orientations of 001 and 111 parallel to the compression axis showed typical dislocation slips in the BCC crystal. However, weak and nearly random texturing seen in the fine-grained DRX sections confirmed the presence of GBS.

3. Cold Working Effect of High Carbon Steel Material

Changes in the ratio of big to tiny precipitates in high-carbon steel (1.0C-1.5Cr-0.31Mn-0.20Si, wt%) may be made to concurrently achieve ultra-high strength and excellent ductility, according to SEM, TEM characterisations and tensile testing. Wang et al. [12] used spheroidization annealing, cold rolling, recrystallisation annealing, and cold drawing, a high yield strength of 670 MPa, tensile stress of 740 MPa, and excellent ductility (elongation of 26%) was achieved. As a result, 1.39 1014 m2 of high dislocation storage in nanosized precipitates with a huge ratio of big size to the tiny size of 0.28 were produced in Figure 3. Also, the cold-rolling process was simulated using the finite element (FE) approach. After the fourth pass of the 0.10C-1.50Cr steel, the maximum stress and strain were 830 MPa and 0.6 at a depth of 3 mm, respectively. Severe plastic deformation and attrition from the rollers may have contributed to the stress and strain buildup in the top layer. This accounted for the development of thick low-angle grain boundaries at the cold rolled steel's surface.

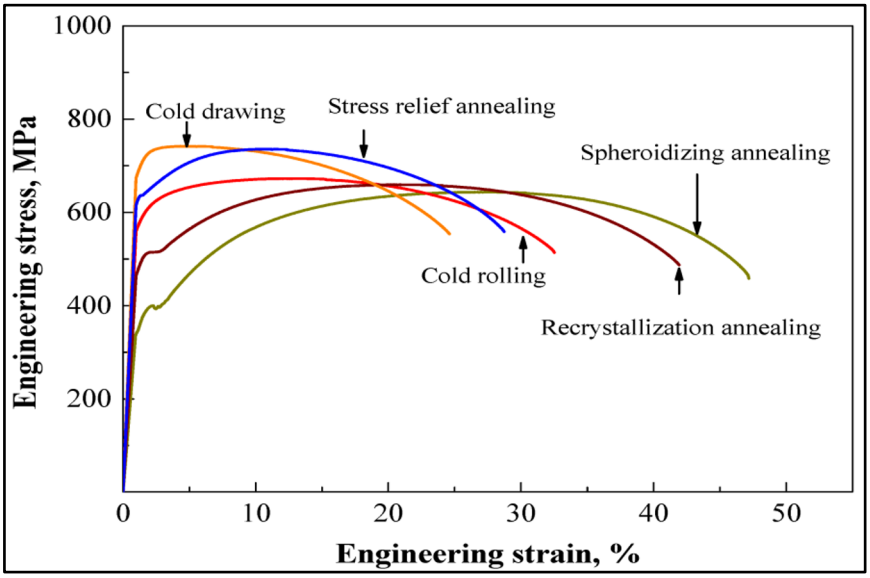

Figure 3. Engineering stress-strain curves of the experimental steel after different processes. [12]

Tkalcec & Mari [13] The study compared the internal friction (IF) spectra for 1.23 weight percent carbon steel with martensitic, bainitic, or ferritic structures and the impacts of cold work. At room temperature, samples with a martensitic structure have a distinctive spectrum with five peaks and an exponential background. The sample structure becomes ferritic after tempering at 800 K. Except for peak P5, recognised as a Snoek-Köster (S-K) relaxation, all peaks are lost, while their amplitudes are significantly diminished. The bainitic structure and the initial ferrite contain the Snoek-Köster peak. However, it has a considerably smaller amplitude than in martensitic samples. A broad double peak forms between 200 and 300 K after cold work, such as bending or roll milling, is applied to tempered samples at room temperature. Initial ferrite that has undergone intense machining exhibits a peak that is comparable to this one as well. A local minimum in the IF spectrum is observed at cold work and post-ageing temperatures. This minimum is the result of carbon precipitates' dislocation pinning. Arioka et al. [14] The incubation period for predicting fracture formation following prolonged exposure to hot water was explored to understand the underlying mechanisms better. Cold-worked carbon steel (ASTM A106 [UNS K03006]) blunt-notched compact tension-type specimens were used for the tests conducted between 320°C and 450°C in hydrogenated pure water and the air. Five significant trends were found. First, intergranular cracking was seen in water and air, even under static stress circumstances and with cold-worked steel specimens. The crack initiation time in an operational plant (Point Lepreau Nuclear Generating Station, Point Lepreau, New Brunswick, Canada) appeared to lie in the extrapolated line of the experimental results, and second, 1/T-type temperature dependencies of initiation times for cold-worked (CW) carbon steel (CW carbon steel) were observed. Finally, before cracks in the water and the air started, cavities were found near the grain boundaries at the bottom of a notch (a highly stressed site). The vacancies condense into cavities, weakening the binding strength at grain boundaries. As a result, it is expected that throughout incubation, the bond strength will decline. Fourth, the pace at which cavities formed in water was more than ten times faster than in the air. This implies that the absorption of hydrogen, which arises from the decrease of water on the surface, may increase the diffusion rate of vacancies. Sixth, stress corrosion cracking (SCC) and creep cracking showed strong correlations between crack propagation rates and cavity creation. Results showed that creating cavities at grain boundaries, both in creep cracking and for SCC in high-temperature

water, is the rate-limiting mechanism of crack expansion. Lastly, the diffusion of vacancies induced by stress gradients was investigated using a specifically developed compact tension (CT)-type specimen to evaluate the mechanism of intergranular stress corrosion cracking (IGSCC) onset and development at high-temperature water. The best explanation for the current data appears to be the creation of cavities from the collapse of vacancies as a model for IGSCC in cold-worked carbon steel in high-temperature water.

Özbek & Saruhan [15] The need for production and ecological efficiency has grown dramatically in recent years as technological advancements have accelerated quicker than ever. New cooling and lubricating methods have supplanted studies examining dry machining and coolant removal. Regarding tool life and worker health, the impacts on surface roughness directly connected to end-product quality are being studied. As a result, the environmentally friendly minimal quantity lubrication (MQL) method is currently used more frequently and is a significant rival to dry and coolant machining. The workpiece for this investigation was made of AISI D2 cold work tool steel, a substance often utilised in the mould industry. Testing was done in dry and MQL conditions and temperature, cutting tool vibration amplitude, tool wear, surface roughness, and tool life were all measured. Three distinct cutting speeds—60, 90, and 120 m/min—and two different cutting tool coating types—CVD (chemical vapour deposition) and PVD (physical vapour deposition)—were used in the trials. Cutting depth and feed rate were kept constant at 0.09 mm per revolution. Compared to dry cutting, the results showed that tool wear, cutting temperature, and cutting tool vibration amplitude were all reduced by 23, 25, and 45%, respectively. These enhancements resulted in an 89% improvement in the workpiece's surface roughness and a 267% increase in tool life. Sathish et al. [16] The main goal of the current study is to explore and evaluate the properties of diffusion bonding, employing Ti-6Al-4V and AISI 4140 Medium Carbon Steel to combine dissimilar materials. ANSYS software is used to analyse temperature distribution and stress intensity. For diffusion bonding, the process variables like time, temperature, and pressure maintained during the process determine the joint quality. Using AISI 4140 Medium Carbon Steel, Diffusion Bonding Experiments for Ti-6Al-4V were conducted by altering the pressure (5 MPa, 10 MPa, and 15 MPa), temperature (750 °C, 800 °C, and 850 °C), and duration (60 min, 90 min, and 120 min). Ansys produced the diffusion-bonded joints and handled the temperature distribution of the Ti-6Al-4V with AISI 4140 Medium Carbon Steel. Man-Tai & Ben [17], examines the material characteristics, residual stress distributions, and cross-sectional behaviour of cold-formed steel elliptical hollow sections. The experimental study includes four cross-section series with nominal section aspect ratios ranging from 1.65 to 3. Tensile coupon tests were used to determine the material characteristics for each cross-section series and the distribution of material properties on half of the cross-section profile of a sample section. In the half-section profile of the same sample section, the distributions of bending and membrane residual stresses in the longitudinal and transverse directions were measured. On five stub column specimens, the initial local geometric defects were measured. Moreover, stub column tests were performed between fixed ends to examine the structural behaviour of cold-formed steel elliptical hollow section stub columns and the material characteristics of the entire cross-section in the cold-worked state. In addition to conducting an experimental inquiry, a finite element model was created and validated using the test findings. This model was then used to conduct comprehensive parametric research that included various cross-section geometries. A formalised design standard for compression members with elliptical hollow sections is not yet. The stub column strengths from the experimental program and numerical analysis were solely compared with the anticipated strengths by the equivalent diameter technique and equivalent rectangular hollow section approach presented by earlier researchers for the design of hot-finished steel elliptical hollow sections, the current traditional design guidelines initially created for a circular hollow

section with equivalent diameter, as well as the Direct Strength method. The comparisons reveal that the Direct Strength Method delivers the most precise and dependable design strength forecasts among the available design approaches, yet there is still room for improvement. The Direct Strength Method and the Continuous Strength Method are modified in this work to increase the goal of increasing the predictability of design strength.

In the work of Dami et al. [18] water atomisation (WA), mechanical milling (MM), and spark plasma sintering was used to create the TiC-reinforced CoCrFeMnNi high-entropy alloy (HEA) composite (SPS). Using electron backscatter diffraction, transmission electron microscopy, and room temperature compression testing, the microstructural development and mechanical characteristics of TiC-reinforced HEA composite are examined. Fine grain size, high yield strength, and high strain hardening were produced by adding 5-weight percent of TiC nanoparticles to CoCrFeMnNi HEA. After sintering, the average grain size obtained for alloys with and without TiC is 5.1 m and 10.6 m, respectively. Without losing ductility, the inclusion of TiC raises the compressive yield strength from 507 MPa to 698 MPa and the compressive fracture strength from 1527 MPa to 2216 MPa. The strengthening behaviour of TiC-reinforced CoCrFeMnNi HEA composite is quantitatively discussed based on grain boundary strengthening, dislocation strengthening, and dispersion strengthening. The role of TiC nano-particles in strain hardening improvement is investigated concerning the dislocation-particle interaction and, consequently, increased dislocation density. Rokilan & Mahendran [19], because of its lightweight nature and quick and simple construction features, cold-formed steel (CFS) is increasingly being employed in building construction worldwide. Nevertheless, the extent of its fire resistance is unclear, which may limit its applicability. A thorough understanding of CFS's increased temperature mechanical characteristics is crucial for fire design objectives. While various important research on the mechanical characteristics of CFS has been carried out, no prediction equation is available to compute the proportional limit stress of CFS at raised temperatures, and the increased temperature reduction factors differ greatly between them. Also, they demonstrate considerable differences between cold-rolled steel sheets and CFS sections' enhanced temperature reduction factors. This study investigated the mechanical characteristics of low- and high-strength cold-rolled steel sheets, high-strength CFS-lipped channel sections, and floor decks under isothermal circumstances at temperatures ranging from 20 to 700 °C. Young's modulus and yield strength prediction equations from AS/NZS 4600 have been confirmed, and additional predictive equations for ultimate strength, stress at 2% total strain, 0.05% proof stress, and proportional limit stress have also been provided. A two-stage stress-strain model was developed to effectively forecast the stress-strain curves of CFS at both ambient and increased temperatures.

Klimova et al. [20], investigated the effects of annealing a cold-worked CoCrFeMnNi alloy at temperatures of 500-900 °C for 1–50 h on the structure and mechanical characteristics. After an hour of annealing, the face-centred cubic (fcc) matrix recrystallised at 600–900 °C, and either a Cr–rich body–centred cubic (bcc) phase or particles from the sigma phase precipitated at 500–700 °C. Moreover, the annealing duration was extended to 50 h at 600 °C, which caused the fcc grains and bcc/sigma particles to continue to develop. In contrast, the sigma phase's percentage increased at the expense of the bcc phase particles. It was discovered that the pinning action of the second phase particles regulated the development of the fcc grains. The strength of the alloy significantly increased after an hour of soaking at 500–600 °C as a result of the second phase’s precipitation. While annealing at greater temperatures and a longer period at 600 °C led to softening, the alloy showed respectably high strength after 50 h of annealing. The latter case's strength was mostly derived from the tiny fcc grains maintained due to the second phase particles' pinning action. According to Kong et al. [21], the peak strengthening for the Cu-rich nanocluster-strengthened high-

strength low-alloy (HSLA) steels is typically achieved by ageing treatments at 400–550 °C. Unfortunately, these temperatures are dangerously close to the temper-embrittlement range of 300–600 °C, which results in low impact toughness. Nevertheless, ageing at temperatures above the embrittlement regime can increase toughness at a significant strength cost. In this study, the processes of strengthening and toughening of a low-cost weldable HSLA steel with low carbon (C 0.08 wt%), nickel (Ni = 0.78 wt%), and copper (Cu = 1.3 wt%) contents were thoroughly examined. Our results demonstrate that the low-C-Ni-Cu HSLA steel is insensitive to the ageing temperatures and can reach yield strength (YS) and ultimate tensile strength (UTS) above 1000 and 1100 MPa, respectively, with tensile ductility > 10% (reduction of area > 60%) at a heat-treat temperature of 640 °C using a variety of strengthening processes. Moreover, by balancing the strengths of the fine grain size (2.5 m), medium-sized (14 nm) overaged Cu-rich precipitates, tempered martensite, and fresh martensite, one can get an excellent low-temperature (40 °C) impact performance (200 J) with high YS (900 MPa) and UTS (1000 MPa) (or carbides). A longer aging process at 640 °C can also result in comparatively lower YS (800 MPa) and UTS (900 MPa), which are beneficial for steel manufacture. Also, based on the dislocation theories in this work, the dislocation-precipitate interactions were investigated.

4. Study of different Heat Treatment techniques for High Carbon Steel Material

DeCost et al. [22], present a microstructure dataset that focuses on intricate, hierarchical patterns discovered in a single piece of Ultrahigh Carbon Steel after undergoing several heat treatments. By applying recent computer vision research picture representations to these microstructures, we explore how supervised and unsupervised machine learning approaches may be utilised to generate insight into microstructural trends and their relevance to processing circumstances. By categorising microstructures according to their principal microconstituent and a subset of the microstructures according to the annealing circumstances that produced them, we analyse and compare key point-based and convolutional neural network representations. We illustrate graphical approaches for exploring microstructure and processing datasets and for comprehending and interpreting high-dimensional microstructure representations using the nonlinear dimensionality reduction and visualisation technique known as t-SNE. Ramakoteswara et al. [23], under dry sliding wear circumstances, the sliding friction and wear behaviour of aluminium matrix composites (AA7075-TiC) have been studied. The aluminium metal matrix composites (AMMCs) are made by stir-casting AA7075 matrix metal and TiC-reinforced particles with an average size of 2 m. In both the cast and heat-treated (T6) regimes, the examined AMMCs included 2–10 weight percent of TiC particles. All composites outperformed the matrix metal in hardness, tensile strength, and elongation percentage in all situations. The 2 m/s sliding speed, 2 km of sliding distance, and 20 N normal load were used in the wear testing. As the weight % of TiC particles in the composites grew, so did their wear resistance. Moreover, the wear rate of the composite material was noticeably lower than that of the matrix material. SEM was used to thoroughly investigate the AMMCs in both their as-cast and T6 conditions to determine the impact of the TiC particles. Compared to their as-cast state, it has been found that both the matrix and the composite significantly improved their mechanical and tribological characteristics under T6 heat treatment conditions. Ramakoteswara et al. [24], to better understand the evolution of martensite tetragonality c/a and phase fraction generated during the transformation, in situ and ex-situ studies were performed on two high-carbon sheets of steel, 0.54 and 0.74 wt pct C, using three different cooling rates: 15 °C/s, 5 °C/s, and 0.5 °C/s. The transformation behaviour was investigated using a combination of in situ high-energy X-ray diffraction under controlled cooling and spatially resolved tetragonality c/a determination by electron backscatter diffraction pattern matching. Stronger auto

tempering is required for a lowering cooling rate and greater Ms, which results in a drop in average tetragonality. The various Ms for the steels also clearly affected the martensitic transformation. The fraction of martensite at room temperature decreased with a slower cooling rate, whereas the fraction of auto-tempered martensite rose. For all cooling rates, a heterogeneous distribution of martensite tetragonality was seen. [25] Selective laser melting (SLM) was used in this study to create Ti6Al4V ELI samples, which were subsequently heated under vacuum (HT) or heated isostatically (HIP). The microstructure was examined using optical microscopy (OM) and scanning electron microscopy (SEM). Columnar grains and acicular ′ martensite was determined to be the dominant components of the as-built microstructure. Thermo-mechanical processes made it possible to change the microstructure in terms of the volume fraction and chemical makeup of the phases, as well as the size and form of the grains. With the phase change, HIP treatment drastically reduced inner flaws like pores and internal fissures. The tensile and fatigue characteristics of the Ti6Al4V ELI samples corresponding to the various microstructures were examined. As-built samples showed strong tensile characteristics but poor ductility, with an average elongation of less than 6% and weak fatigue resistance. HT samples showed lower tensile strength but better elongation behaviour and considerably increased fatigue resistance compared to as-built samples. Because to the removal of internal flaws, the HIP treatment also caused a decrease in strength but also enhanced ductility and fatigue behaviour Compared.

Fuat et al. [26], studied the effects of deep cryogenic processing and tempering on surface roughness and tool wear when hard-turning AISI D2 cold work tool steel. How deep cryogenic procedures affected mechanical characteristics (macro and microhardness) and microstructure were investigated. Conventional heat treatment (CHT), deep cryogenic treatment (DCT-36), and deep cryogenic treatment with tempering were three sets of test samples that were analysed (DCTT-36). The samples in the first group only underwent CHT up to a hardness of 62 HRc. Following standard heat treatment, the second group (DCT-36) underwent processing for 36 hours at 145 °C. The second group (DCTT-36) had undergone deep cryogenic and standard heat treatment, followed by two hours of tempering at 200 °C. Cutting tools made of Al2O3 + TiC matrix-based TiN-coated ceramic (AB2010) and Al_2O_3 + TiC matrix-based untreated mixed alumina ceramic (AB30) were also employed in the studies. Based on cutting speed, cutting tool, workpiece, depth of cut, and feed rate, artificial neural networks (ANNs), a type of artificial intelligence technique, were utilised to assess the surface roughness. The conventional back-propagation technique was discovered to be the best option for training the model for artificial neural network modelling. Three distinct feed rates (0.08, 0.16, and 0.24 mm/rev), three different cutting speeds (50, 100, and 150 m/min), and three different cutting depths (0.25", 0.50," and 0.75") were chosen. Tool wear trials were conducted with a cutting speed of 150 m/min, a feed rate of 0.08 mm/rev, and a cutting depth of 0.6 mm. The trials showed that the DCTT-36 sample produced the best tool wear and surface roughness outcomes. When cutting tools were compared, the coated ceramic tool had the best outcomes for tool wear and surface roughness (AB2010). The DCT-36 had the highest results for both macro and microhardness. The DCTT-36 sample had the greatest results from a microstructural perspective, with uniform and thinner secondary carbide deposits. Isil et al. [27] created a biomass-based activated carbon using $ZnCl_2$ as an activation agent during chemical activation. A portion of the activated carbon sample underwent a single-step heat treatment again at 800 °C in an inert environment. Both the untreated and heat-treated carbon samples underwent testing as supercapacitor electrode materials. The surface characteristics of the carbon sample were dramatically impacted by further heat treatment, additionally, despite having a smaller specific surface area, both aqueous and organic electrolytes significantly improved electrochemical performance. The organic electrolyte-based supercapacitor device has a greater rate capability than the aqueous

one (KOH). The organic electrolyte-based supercapacitor device was scaled up from coin to pouch size while maintaining the electrochemical response. It was made from a heat-treated sample. Across 10,000 cycles, both coin and pouch supercapacitors demonstrated high capacitance retention. This is equivalent to industrial supercapacitors with high-rate activated carbon bases.

Alireza et al. [28], a normally rolled low-carbon, low-alloy shipbuilding steel plate (EH36) will be used in this study to examine the viability of fabricating it utilising the developing wire arc additive manufacturing (WAAM) technology using ER70S feedstock wire. After the manufacturing stage, both traditionally rolled and WAAM samples underwent various heat treatment cycles, including air-cooling and water-quenching from the inter-critical austenitising temperature of 800 °C. Before and after various heat treatment cycles, the microstructural and mechanical characteristics of rolled and WAAM-fabricated ship plates were thoroughly evaluated and compared. The microstructure of the rolled ship plate underwent hard martensite-austenite (MA) constituent development as a result of both air-cooling and water-quenching heat treatments, increasing the component's hardness and tensile strength and decreasing its ductility. However, it was discovered that the WAAM ship plate's microstructure was homogenised during the air-cooling heat treatment, which resulted in a slight loss of hardness and tensile strength. In contrast, the water-quenching cycle produced acicular ferrite and intergranular pearlite, which improved the part's mechanical properties. The improved mechanical integrity of the water-quenched WAAM component compared to its rolled equivalent confirmed the viability of the WAAM's manufacturing of the ship plates. Yuka et al. [29], selective laser melting (SLM) has drawn much interest as a cutting-edge technique for creating biomedical devices. However, because of the quick heating and cooling, items made by SLM are prone to accumulating significant quantities of residual stress, which is bad for their mechanical qualities. To reduce residual stress and enhance their mechanical characteristics, Co-Cr-Mo alloy specimens for this investigation were made using SLM and subsequently heated to a range of temperatures (750, 900, 1050, or 1150 °C). The mechanical characteristics of the produced specimens were assessed using tensile and Vickers hardness tests. At the same time, the alloy microstructure was examined using confocal laser scanning microscopy, scanning electron microscopy coupled with energy-dispersive X-ray spectroscopy, electron backscattered diffraction, and X-ray diffraction techniques. According to the results, raising the alloy's heat-treatment temperature from 750 °C to 1150 °C boosted ductility while lowering Vickers hardness and offset yield strength by 0.2%. All heat-treated specimens produced the phases, and as the heat-treatment temperature increased, the volume percentage of the phase dropped. The recovery began when the specimens were heated to 750–1050 °C and progressed as the temperature rose; the residual stress in the examined specimens was not substantially alleviated. The formation of equiaxed grains and the dramatic relief of the residual stress, along with an increase in the specimen's elongation and a decrease in its strength (as compared to those of the other heat-treated specimens), were observed simultaneously after heating to 1150 °C, indicating that the specimen completely recrystallised and that the residual stress was the catalyst for this recrystallisation. As a result, reducing the residual stress with heat treatment at 1150 °C for 6 hours results in a homogenised microstructure and acceptable ductility.

Yuka et al. [30], examined how post-tempering heat treatment affects the stability of retained austenite and hardness in dual-phase high-carbon steel. This impact was examined by focusing on the micro- to nano-scale stability of the remaining austenite and the nanomechanical characteristics of the individual grains. Austenite au, in dual-phase high by maintaining equal processing conditions throughout, samples with and without post-tempering heat treatment were prepared in this investigation. Microstructural examinations,

hardness tests, and compression tests were performed for both samples to determine the characterisation of various phases. Due to the displacement of C content within the grains, tempering impacted the dislocation density and the deformation mechanism of phases. Tempering made it easier for carbon to diffuse from martensite to residual austenite and for nano carbides to develop in the martensite matrix, reducing its toughness. The material's total hardness was reduced by 16%. Nevertheless, tempering considerably improved the stability of residual austenite at the nano and bulk scales. These findings provided crucial insight for creating low-alloyed, high-carbon steel for industrial use. Lv et al. [31], after cyclic heat treatment, the spheroidizing behaviour of cementite in steel with a Fe-0.8C mass% was examined. The impact of cyclic numbers was studied on the microstructure and mechanical characteristics of the experimental steel. Each cycle heat treatment in the current study consisted of a brief (5 min) hold time at 1043 K (above A1 temperature 1003 K) and a brief (3 min) hold time at 953 K. With a rise in cycle numbers, both the cementite's spheroidizing ratio and the average particle size increase. The cementite entirely spheroidizes after five heat cycles, with an average particle size of 0.49 m and a bigger particle ratio of less than 4%. The experimental steel's plasticity rises after cyclic heat treatment. The specimen's transformed elongation is around 8%, the specimen elongation after one cycle is 25.4%, and the elongation after five cycles peaks at 33.9%. The ultimate tensile strength (UTS) of the as-transformed specimens is around 680 MPa, and it drops to approximately 620 MPa for the 1-cycle specimen; however, it rises to approximately 650 MPa for the 3-cycle specimen. After cyclic heat treatments, the yield strength to tensile strength ratio is around 0.70.

5. Annealing and normalising method heat treatment for High Carbon Steel Material

To prevent oxidation, the whole heat treatment process was done in a tube furnace filled with Aar gas, and the initial microstructure was normalised ferrite pearlite [32]. Using Thermo-calc Soft, a thermodynamics calculation, the critical temperature was examined. While comparing the mechanical characteristics of three different heat treatment cycles, the alloy-steel sample that underwent inter-critical annealing with the highest elongation rate revealed a spheroidized structure. Also, the impact of alloy-steel holding duration during inter-critical annealing was examined. The findings demonstrated that carbide decomposition increased with holding time. The findings of the hardness test also revealed that the hardness value did not vary appreciably between the inter-critical annealing cycle's first five and ten hours. The best microstructure and mechanical properties were obtained by repeating the inter-critical annealing cycles three times when they were used to examine the effects of repeated frequency heat treatment cycles. Various mechanical qualities are necessary for many industrial applications, especially suspension systems, to match the designer's requirements [33]. In the current study, LIBS calibration curves were employed for the first time to determine the hardness (HV units) of the light-duty low-carbon spring steel DIN50Cr3 using a semi-nondestructive method. Three different spring steel samples, DIN50Cr3, were effectively treated for this purpose by being put through various treatment regimens, including R1 annealing, R2 quenching, and R3 normalising. Microstructural investigations and calibration curves based on the Vickers mechanical hardness and the ratio of ionic to atomic line intensities in LIBS spectra were carried out. The mechanical hardness for spring steel DIN50Cr3 that was put through various tempering heat treatment regimes R4, R5, and R6 is then inferred from the calibration curves, and their values were correlated with those obtained from the Vickers test. Scanning electron microscopy (SEM) was used to perform microstructural analysis, and the correlation between the variation in the measured hardness level and the microstructural alterations brought on by each heat treatment regime was established. As shown in the Figure5 below

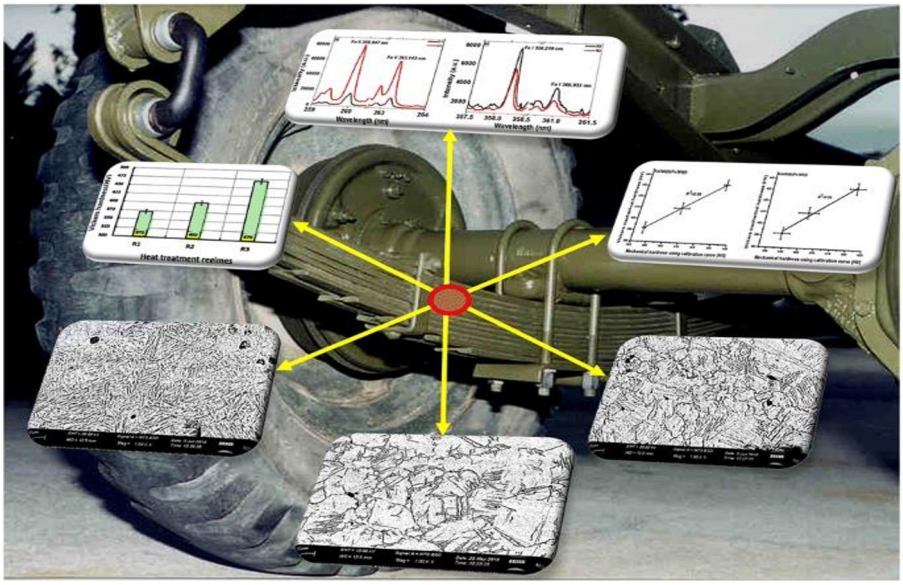

Figure 4. shows heat treatment, microstructure analysis and other related graphical illustrations [33].

Kosturek et al. [34], investigated Inconel 625 and steel P355NH were welded together explosively. A bimetal clad plate that had been explosively welded was put through two distinct post-weld heat treatment procedures: stress relief annealing (620 °C for 90 min.) and normalising (910 °C for 30 min.). Microhardness tests, EDS analysis methods, light and scanning electron microscopy, and other techniques have all been used to assess the impact of heat treatments on the joint's microstructure. It has been claimed that stress relief annealing partially causes the steel P355NH microstructure in the joint zone to recrystallise. In addition to both materials recrystallising simultaneously, normalisation also led to the production of precipitates and a diffusion zone in Inconel 625. Chromium- and molybdenum-rich M23C6 and M6C carbides have been found as the two forms of precipitates in Inconel 625. According to reports, voids also arise due to the diffusion of alloying elements into steel P355NH along grain boundaries. According to grain microstructure analysis using a scanning transmission electron microscope in Figure 4, the diffusion zone contains columnar and equiaxed grains alongside Inconel 625 alloy (at the side of steel P355NH). As shown in Figure 5.

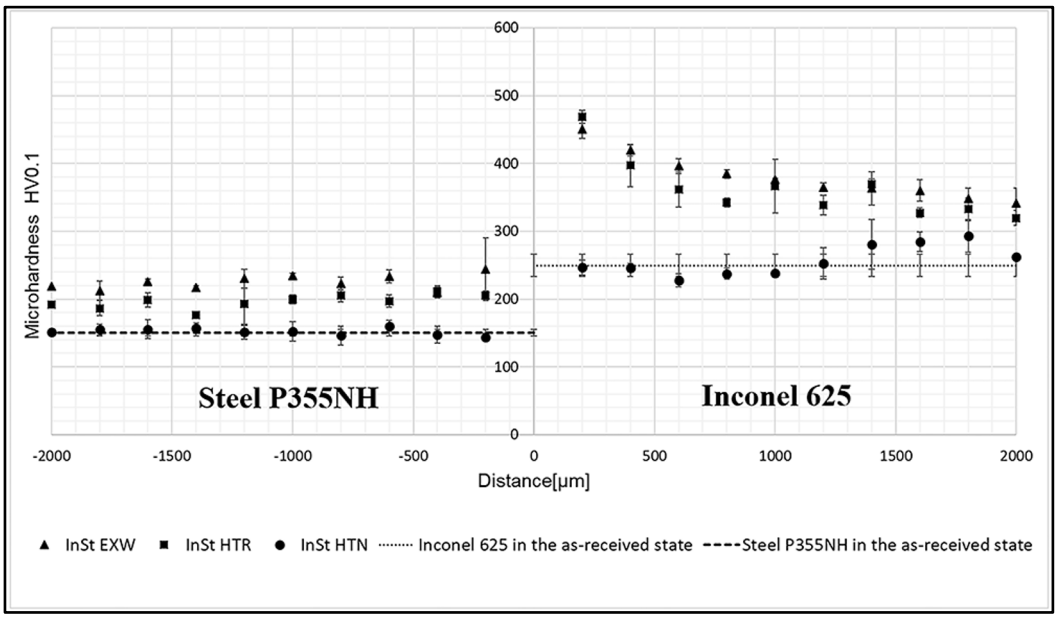

Figure 5. the microhardness analysis's findings [34]

According to Sivam et al. [35], heat treatment is one of the most popular methods for getting the desired mechanical characteristics in metal alloys, which modifies the second phases or the microstructure, namely the grain, in heat-treatable alloys. Sometimes materials that have been treated go through further procedures, including forming, machining, welding, etc. As a result, the current study addresses the impact of heat treatment on AISI 1050 steel and the resulting microstructural modifications that link them to mechanical behaviour. In manufacturing actuators, landing gear, bearings, and structural parts for the aircraft industry, AISI 1050 steel is often utilised. In this investigation, several AISI 1050 steel samples underwent annealing, normalising, or spheroids after being heated to a temperature above the austenitic area. The AISI 1050 steel's characteristics may be easily changed by heat treatment to fit a specific purpose and for further processing, which is suggestive. Microstructural grain size, yield strength, tensile strength, hardness, and % elongation is among the properties compared. The outcomes, therefore, give a better understanding of the method for AISI 1050 steel's demanding use in aircraft structural applications and associated mechanical processing. Heat treatment increased grain size, decreased strength and hardness, and enhanced attributes more suited for machining and forming. Also, Adnan et al. [36] say the effect of heat treatment on the corrosion behaviour of API 5L X65 pipeline steel in the presence of acetic acid HAc and carbon dioxide CO_2 environment was investigated experimentally. One of the corrosion hazards that might cause a loss of pipeline integrity has been identified as CO_2 corrosion. The specimens used in this study were obtained from X65 steel pipes and were put through the appropriate heat treatments, including annealing, normalising, and quenching. Specimens that were received as received served as a control. A three-electrode glass cell setup was used for CO_2 corrosion tests, both with and without acetic acid. Weighing loss and linear polarisation resistance (LPR), electrochemical techniques were used to calculate corrosion rates. The findings demonstrated that heat treatments had an impact on corrosion rates. In contrast to other examples, quenched specimens seemed to corrode more quickly than annealed ones. All heat-treated specimens' corrosion rates were usually accelerated by the presence of acetic acid in an aqueous CO_2 atmosphere. Rajendran et al. [37], a strong joint is formed during friction welding when the process variables are

optimally combined. Depending on the material combination and treatment settings, metallic changes occur. The joints can be identified using mechanical testing, macroscopic and microscopic studies. Studies are conducted on a friction-welded joint constructed of mild steel AISI 1010 and high-carbon high-chromium steel D3 to develop a functionally graded tooling element. Post-weld heat treatment has been tried to improve the joint's quality, and the experiment produced some intriguing outcomes. Comparing annealed specimens to unheated specimens, the mechanical strength and microhardness of the joint increased by 16% and 14%, respectively. Using optical and scanning electron microscopes, EDX, and XRD studies, the structural specifics and components of fusion lines and heat-affected zones were investigated. Heat treatment might convert the deformed metastable phases (austenite and untempered martensite) into joint materials with a more refined structure and composition close to the fusion line. It is anticipated that this would lengthen the useful life of friction-welded components. Sebayang et al. [38], the impact of quenching, normalising, and annealing on changes in hardness, tensile strength, and microstructure of tool steel AISI 01 when the material goes through a heat treatment procedure is covered in this paper. This heat treatment procedure involves a 600° C initial warming step, a 5-minute detention period, and then 850° C austenitisation heating. A separate cooling method was used, which included annealing, normalising, and quenching SAE 40 oil. Tensile, hard, and microstructure tests and SEM shooting (Scanning Electron Microscope) are conducted. This is done to examine the impact of various heating and cooling techniques. The study's findings are differences in tensile test value, hardness, and microstructure due to the effect of the various processing differences. Because the beginning material does not undergo a heat treatment, the quenching process yields the greatest tensile and hard values, followed by the normalising process, annealing, and the starting material, which has the lowest values. The resultant microstructure is either pearlite or cementite, depending on the particle size and form. The harder something is, the bigger the grain size is.

Gebril et al. [39] studied several austenitic phases (850, 900, and 950 °C) and holding durations (30 min. and 1 h.) are considered as part of the heat treatment of 0.75% carbon steel with 4.50% Mo. At 850 °C, there is no discernible rise in hardness, but at 900 °C, both oil- and water-quenched specimens exhibit a change in hardness values. At 950 °C, all quenching media, including air and furnace cooling, showed a considerable change in hardness values. The samples' hardness rises as the austenitisation temperature rises, particularly for samples chilled with oil and water at 950 °C. Testing revealed that the microstructures include carbides. Despite melting at 1,050 °C, the carbides did not entirely melt because of the molybdenum content, which creates durable carbides until melting. Cao et al. [40] created micro-nanostructured anodised iron oxide films by combining heat treatment and anodisation. By applying heat to the substrate to change the location of the cementite and ferrite, it was possible to shift these oxide layers at the micron scale. The amount and types of carbon present in cementite and ferrite affect the anodisation's shape. It was discovered that annealing iron oxide at 300 °C can increase its crystallinity while preserving its original micro-nano structure. Higher annealing temperatures would cause the collapse of nano-porous structures and the rebuilding of the surface morphology, even though the crystal quality of iron oxide might still be enhanced. Moreover, samples that have been anodised from materials with cementite and lamellar ferrite have improved specific capacitance. At a scan rate of 20 mV/s, the iron oxide coating on the annealed substrate in our samples had the maximum specific capacitance of 35.3 mF/cm^2. Brian [41] presented a microstructure dataset focusing on intricate, hierarchical patterns discovered in a single piece of Ultrahigh Carbon Steel after undergoing several heat treatments. The study explores how supervised and unsupervised machine learning approaches may be utilised to generate insight into microstructural trends and their relevance to processing circumstances by applying recent

computer vision research picture representations to these microstructures. By categorising microstructures according to their principal microconstituent and a subset of the microstructures according to the annealing circumstances that produced them, we analyse and compare key point-based and convolutional neural network representations. They illustrate graphical approaches for exploring microstructure and processing datasets and for comprehending and interpreting high-dimensional microstructure representations using the nonlinear dimensionality reduction and visualisation technique known as t-SNE.

6. Hardening and austempering method for heat treatment analysis of High Carbon Steel Material

The hot press forming process creates an automobile flex plate mounted in the engine and transfers torque to the transmission. Myoung-Gyu et al. [42] used the method for quenching of heated high-carbon SK5 steel sheets to significantly boost strength while achieving greater dimensional stability following high-temperature press forming. The indirect approach with a pre-forming stage and direct oil quenching is used to achieve a uniform and quick cooling rate while considering the SK5 steel's cooling properties and the substantial thickness of the flex plate. Austempering and quenching with nitrogen are two commonly used heat treatments studied to create a new tool design for the hot press forming process—thermal treatments for tempering. The goal product, which fulfils two key manufacturers' specifications: high hardness and good dimensional accuracy, may be effectively created by introducing specified tools and chosen heat treatment conditions. Moreover, finite element analysis explains the thermo-mechanical behaviour of hot press-formed sheets and considers transformation-induced plasticity (TRIP) during phase changes. The research confirms that phase transitions are important in lowering dimensional change by undergoing extra plastic deformation during phase transformations and strengthening by altering the hard martensitic phase. In most cases, annealing generates homogeneous tensile characteristics in cold-rolled BCC metals. These components' ultimate microstructure is frequently described as having a somewhat coarse microstructure and inferior tensile characteristics [43]. The rolled microstructure and crystallographic texture advantages can be maintained as the microstructure is homogenised by cross-rolling. The study examined how cross-rolling and austempering heat treatment affected the mechanical characteristics of the AISI 8670 steel sheets. The effectiveness of the novel deformation and heat treatment strategy was measured against the traditional production techniques. According to the findings, cross-rolling combined with low-temperature austempering results in consistent strength of fibre textures and homogenous lower bainitic microstructure, which produce desirable isotropic mechanical characteristics. With the novel deformation route and heat treatment combination, systematic increases in UTS and toughness of 40% and 57% were achieved. Sourmail et al. [44] Dilatometry and salt-bath heat treatments examine the effects of austempering, quenching, and tempering on high Si hyper-eutectoid steels. Using X-ray diffraction, changes in retained austenite content are quantified. Findings are compared to published data and the dominant explanation for bainite generation. A unique heat treatment that is technologically equivalent to quenching and tempering is developed from retained austenite development during tempering, except that the rules governing the selection of tempering temperature and time are different. It has been demonstrated that this heat treatment produces an alloy class-unique combination of hardness, preserved austenite content, and thermal stability. Also, this outcome is obtained for periods of heat treatment that are thought to be usual. It has been demonstrated that low-temperature austempering requires much longer holding times to produce somewhat lower combinations of hardness and residual austenite contents shown in the Figure 6.

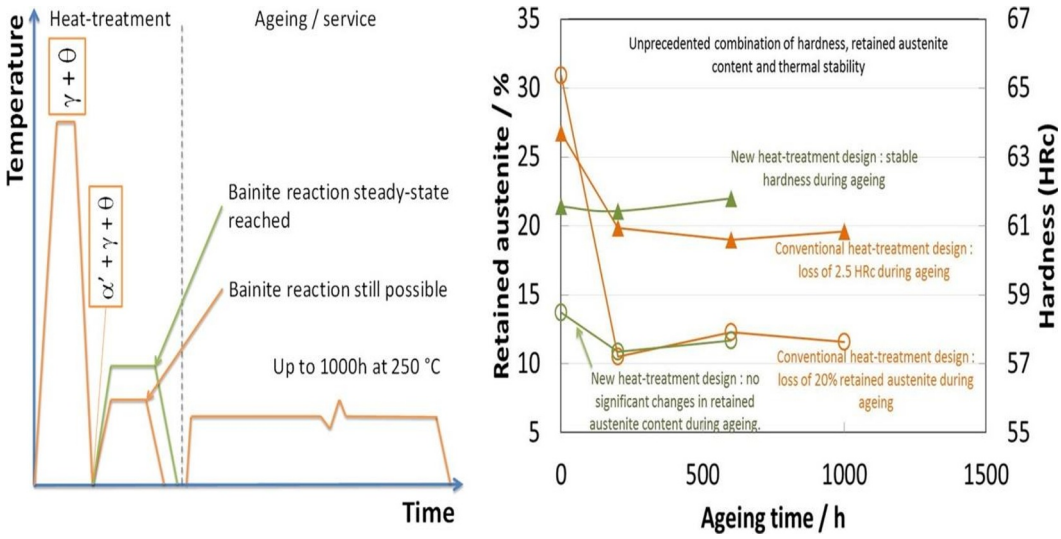

Figure 6 : heat treatment.[44]

According to Behzad et al. [45], if better mechanical qualities are required in high-performance nanostructured bainitic steels, it is imperative to minimise the thermally and mechanically less stable austenite blocks. In this case, step-austempering might be a useful technique. This paper examines the strength-ductility-impact toughness combinations in nano-bainite following a two-step austempering procedure compared to those obtained by a traditional isothermal bainite transformation. It has been demonstrated that following the step-austempering procedure, which reduced the average volume percentage of austenite, enhanced its mechanical stability, and polished the final microstructure, massive austenite blocks further disintegrated to bainite. Step-austempering improved the yield strength and ultimate tensile strength qualities while raising the hardness value. At the early stages of the second step of transformation, the higher elongation level and enhanced impact toughness were also a result of the retained austenite's stronger mechanical stability in step-austempered samples. The significant discovery that the second stage of austempering's transformation time had an impact on the properties of ductility and toughness supported the theory that, in addition to mechanical stability and morphology of retained austenite, the volume fraction of retained austenite must also be considered when applying a multi-step austempering heat treatment to nano bain steels. Masoud et al. [46] assessed how the temperature and time of the austempering process affected the mechanical characteristics, fracture mode, phase equilibrium, and microstructural evolutions of weld metal in Hadfield steel joints. To do this, shielded metal arc welding (SMAW)-prepared Hadfield steel weld joints underwent the austempering process at 500, 600, and 700 °C for 15 and 30 min. The microstructural and phase evolutions of the weld metals were assessed using the optical microscope (OM), scanning electron microscope (SEM), transmission electron microscope (TEM), energy dispersive spectroscopy (EDS), and X-ray diffraction spectroscopy (XRD). Tensile, Charpy, and Vickers microhardness tests were used to analyze the mechanical characteristics of the weld joints. SEM also identified the fracture mechanism of the broken surfaces following tensile and Charpy tests. The study's findings demonstrated that lengthening the austempering process' time and temperature increases the yield strength, tensile strength, microhardness, pro-eutectoid (Fe, Mn)3C carbide content, and reduces the size of Austenite grains, a material's capacity for plastic deformation, fracture energy, and the likelihood of ductile fracture in the weld metal of Hadfield welding joints. Ozioko et al. [47], to align the process outputs with the suggested applications, simulation models for predicting the

austenitising temperature and quench time to achieve desired properties of the medium and high carbon steels during their austempering with bitumen-palm kernel oil quenching medium were developed in this study. The models were created using the response surface approach, and its predictors include the kind of carbon steel being treated and the intended area reduction, percentage elongation, ultimate tensile strength, and impact strength. The created models and their terms showed P-values of less than 0.05 and a generally negligible lack of fit status, indicating a more than 95% prediction accuracy. According to the function analysis, the austenitising temperature and quench time needed to achieve any particular set of properties for carbon steel using this heat treatment process are significantly influenced by the main effects and some interactions of these predictors, as well as the quadratic effect of hardness. Thus, the simulations are advised for efficient logistic planning and development in the medium and high-carbon steel-producing industry.

Dongyun et al. [48] The bainitic transition can be accelerated at low temperatures using the two-step austempering procedure. However, the first step in regulating rules is yet unknown. The impacts of the first-step transformation on the bainitic transformation, microstructural evolution, and associated mechanical characteristics of ultra-fine bainitic steel produced by two-step procedures are thoroughly examined in this work. According to the results, the two-step austempering procedure significantly speeds up the bainitic transformation, with a maximum decrease in overall transformation time of 93.1% possible when the first-step bainitic percentage is held constant at 22%. The two-step austempering samples had lower blocky retained austenite and bainitic ferrite plate thickness and length than the typical first-step austempering sample. Even though the two-step austempering samples' hardness and strength are slightly lower than the conventional one-step samples', they still satisfy the product's requirements for bearing, particularly the sample with 22% and 50% first-step fractions, which achieve higher toughness and yield strength, respectively. The process design of ultra-fine bainitic steel is theoretically supported by this study, which is based on an expedited heat treatment procedure, an improved microstructure, and superior mechanical characteristics. Skołek et al. [49] created nano bainite devoid of carbides, and it was necessary to analyse the microstructure and characteristics of cast steel following austempering heat treatment. Using cast steel samples, dilatometric measurements of phase change kinetics were made to order to develop heat treatment settings. This research made creating a time-temperature-transformation diagram and determining the heat treatment settings feasible. The best heat treatment settings were then selected after this. Austenitising was the first step in the heat treatment process, which was followed by an isothermal halt at the temperature where the bainitic transition took place and a final quenching at room temperature. To create nano bainite devoid of carbides, it was necessary to analyse the microstructure and characteristics of cast steel following austempering heat treatment. Using cast steel samples, dilatometric measurements of phase change kinetics were made to order to develop heat treatment settings. This research made creating a time-temperature-transformation diagram and determining the heat treatment settings feasible. The best heat treatment settings were then selected after this. Austenitising was the first step in the heat treatment process, which was followed by an isothermal halt at the temperature where the bainitic transition took place and a final quenching at room temperature. The observations showed that the heat treatment created a highly refined multiphase microstructure and that this microstructure depended on the austempering time. The produced microstructures supplied high tensile strength. However, toughness was considerably influenced by the applied heat treatment settings. Bernardo et al. [50] incorporated bainite as a whole or a partial replacement for martensite is a viable choice for the combination of high strength and toughness, primarily desired by the aerospace and high technology industries. Thermomechanical processing produces high-carbon, carbide-free bainitic steels with a final

bainitic ferrite microstructure and preserved austenite. Compared to normal quenched and tempered steels, these steels' fracture toughness may be reduced by carbides. This article compares the microstructure and impact resistance of four high carbon steel alloys with different amounts of nickel, silicon, and manganese after they were austempered at 280 °C for 12-hour intervals, 24 hours, 72 hours, and 168 hours. These alloys were austenitic at 870 °C and austempered. As a result, the microstructural traits and their morphological and kinetic features were established by assessing the mechanical properties from Rockwell C hardness tests. Typically, the hardness values decrease in the four alloys because stress relief from the austempered treatment caused the bainitic microstructure to have bigger lath forms, decreasing the hardness values in the impact test. SEM fractographic analysis of the samples revealed three stages of the phase transformation: bainitic ferrite and retained austenite formed a microstructure due to the stasis of the bainitic reaction; multiphase microstructure made up of bainitic ferrite, martensite, and retained austenite; and martensitic microstructure. Due to the instability of the austenite, which caused the alloys to absorb energy at slower rates in the beginning (from 24 hours on), an increase in the alloys' capacity to absorb energy—known as plasticity—was formed as a result of the energy lost during the Charpy test's impact. As austenite transforms into martensite, the transformation-induced (TRIP) phenomenon occurs, favouring higher ductility. As a result of the combined action of a failure micromechanism, it was discovered that alloy (a), with a lower concentration (%) of nickel, has a predominance of brittle fracture. For alloy (c), which has a larger percentage of nickel, the primary fracture is also of the brittle type and has tiny microcavities typical of alveoli. The impact of treatment time, which does not affect the failure mechanism and remains brittle until the end for alloys (a), alloy (b), and alloy (c), is another crucial factor to take into account (c).

This section summarises the review of selected literature concerned with the hot and cool working process on high-carbon steel. This summary is debited in Table 1

Table 1: summary of some selected literature for under cool and hot working process of high carbon

Author Details	High-Carbon Steel Used	Heat Treatment	Method of Fabrication	Result
Pillai et al. [51]	A2 steel	Cold working	Machine learning technique SVM	During the development of carbides and phase shifts, the proportion of carbon and its impact mostly pulls the TTT curves.
Z.Q, et al. [52]	Fe–0.8C mass% steel	Cyclic heat treatment	Grains refinement	Lamellar cementite () spheroidizes quickly, and submicron () particles are produced in Fe-0.8C steel under cyclic heat treatments without deformation. The experimental steel's ductility rises visibly, and its strength marginally after cyclic heat treatment.
Zambrano et al. [53]	Fe-Mn-Al-C steel		It was performed at temperatures between 900 and 1150 °C and strain rates ranging from 0.01 s^{-1} to 1 s^{-1}.	The stress-strain curves exhibited typical dDRX behaviour, with a single peak stress and gradual softening. Analysis of the hardening rate versus stress plots and SEM-EBSD measurements evidenced the occurrence of dDRX.

Prusty et al. [54]	High carbon steel	Hot deformation	single hit hot compression experiments at various strain rates and temperatures on two grades of carbon steel together with the Avrami type kinetics equation and Bergstrom approach have been utilised	the presence of carbon increases the dynamic recovery rate at low strain rates due to its effect on the dislocation climb and self-diffusion rate. At higher strain rates, it decreases the rate of dynamic recovery.
Petković et al. [55]	0.68% C steel	Hot deformation	Interrupted compression tests were used to study the static softening of austenite at temperatures from 780 to 1040°C. Prior training was carried out at strain rates in the range 10^{-3} to 10^{-1} s^{-1} and interruption strains of up to 0.41	The results indicate that a critical strain is required to initiate static, i.e., classical, recrystallisation after prior hot deformation. For strains inferior to this critical amount, recrystallisation does not occur at all, even after holding intervals of 10^5 s or more, and softening takes place instead entirely by static recovery.
Chandramouli et al [56]	both 0.35% and 0.65% carbon steel	Cold forming	cold axial deformations	At relatively lower levels of axial deformation, rings subjected to the most severe flow constraint of fully restrained radial flow exhibit the highest densification rate.
Okonkwo et al. [57]	AISI D2 STEEL	Cold forming	The ball-on-disc CSM High-Temperature Tribometer is used (commonly referred to as pin-on-disc tests)	The amount of material deposited onto the disc surface during the wear testing provides conclusive evidence that adhesive wear is predominant for all sliding speeds evaluated. Particularly, the degree of adhesive wear is greatest at the slowest sliding speeds.
Hentschel, et al. [58]	60CrMoV18-5 (1.2358)	Cold forging	LMD	The samples have a dendritic microstructure with fine grains, and their average microhardness is 800 HV 30 HV (or roughly 63 HRC). The microhardness can be slightly increased by preheating the tool steel

				substrates to extra temperatures between 300 and 400 °C.
Ezatpour et al. [59]	K310	Hot deformation	hot compression tests in the range of 900-1100 °C with strain rates of 0.01, 0.1 and 1 s^{-1}	According to the microstructural findings, peak strain, peak stress, and activation energy for dynamic recrystallisation decreased with increasing temperature (low Z) and lowering strain rate. In the meantime, graph analyses revealed that the necklace structure is evolving, and the grain size is decreasing.
Kumar et al. [60]	SKD-11	Cold worked steel	Dry sliding tribological test	The results showed that both sheets of steel exhibited similar wear behaviour at low sliding velocities and low applied loads, however as sliding velocities increase beyond 0.20 m/s, the specific wear rate of SKD-11 steel likewise rises.

7. Conclusions

The study of the effect of hot and cold working on high-carbon steel reveals important insights into the material's microstructural changes and mechanical properties. Hot working improves formability, toughness, and ductility, while cold working increases strength and hardness but reduces ductility and toughness. To optimise the performance of high-carbon steel, further research should focus on characterising microstructural changes, optimising mechanical properties, exploring post-processing techniques, investigating fracture and fatigue behaviour, and assessing industrial applications. The study has the following conclusions:

i. the Impact value obtained after hot rolling is higher than that of cold rolling (It is generally expected that hardness obtained from cold, the Impact value of cold bending is higher than that of hot bending and the Impact value of cold squeezing is higher than hot squeezing.
ii. Cold working produces strain hardening and changes the grain structure, resulting in higher strength but perhaps decreased ductility and toughness, whereas hot working refines the microstructure and enhances the mechanical characteristics of high-carbon steel

8. Recommendations

Based on the study of the effect of hot and cold working behaviour on high-carbon steel, the following recommendations can be made for further research and practical applications:

i. Characterize microstructural changes: Conduct a detailed investigation into the microstructural changes occurring during high-carbon steel's hot and cold working. This can involve advanced microscopy techniques such as electron and X-ray diffraction to analyse grain structure evolution, dislocation density, and other microstructural features. Understanding the relationship between processing parameters and microstructure will provide insights into the resulting mechanical properties.
ii. Mechanical property optimisation: Explore strategies to optimise the mechanical properties of high-carbon steel based on the desired application. Investigate the effect of various hot and cold working parameters, such as deformation temperature,

strain rate, and degree of deformation, on the material's strength, hardness, ductility, and toughness. This will enable the development of processing routes that balance the trade-off between strength and ductility, ensuring the material meets the specific performance requirements.

By addressing these recommendations, further advancements can be made in the understanding and application of high-carbon steel subjected to hot and cold working. This knowledge will contribute to developing improved processing techniques and designing high-performance components using high-carbon steel in diverse industries.

References

1. De Cooman, B. C., Chin, K. G., & Kim, J. (2011). High Mn TWIP steels for automotive applications. *New trends and developments in automotive system engineering*, (1), 101-128.
2. Kadhim, Z. D. (2016). Effect of quenching media on mechanical properties for medium carbon steel. International Journal of Engineering Research and Application, 6(8), 26-34.
3. Drozd, K., Walczak, M., Szala, M., & Gancarczyk, K. (2020). Tribological behavior of AlCrSiN-coated tool steel K340 versus popular tool steel grades. Materials, 13(21), 4895.
4. He, G., Zhao, Y., Gan, B., Sheng, X., Liu, Y., & Tan, L. (2020). Mechanism of grain refinement in an equiatomic medium-entropy alloy CrCoNi during hot deformation. Journal of Alloys and Compounds, 815, 152382. https://doi.org/10.1016/j.jallcom.2019.152382
5. Murugesan, M., & Jung, D. W. (2019). Johnson Cook material and failure model parameters estimation of AISI-1045 medium carbon steel for metal forming applications. Materials, 12(4), 609.
6. Holzweissig, M. J., Taube, A., Brenne, F., Schaper, M., & Niendorf, T. (2015). Microstructural characterization and mechanical performance of hot work tool steel processed by selective laser melting. Metallurgical and Materials Transactions B, 46, 545-549. https://doi.org/10.1007/s11663-014-0267-9
7. Zhiqiang Wu, Yubo Tang, Wei Chen, Liwei Lu, Eric Li, Zhichao Li, Hua Ding, Exploring the influence of Al content on the hot deformation behavior of Fe-Mn-Al-C steels through 3D processing map, Vacuum, Volume 159, 2019, Pages 447-455, ISSN 0042-207X, https://doi.org/10.1016/j.vacuum.2018.10.079.
8. Kumar, S., Maity, S. R., & Patnaik, L. (2020). Friction and tribological behavior of bare nitrided, TiAlN and AlCrN coated MDC-K hot work tool steel. Ceramics International, 46(11), 17280-17294. https://doi.org/10.1016/j.ceramint.2020.04.015
9. Mohammad Hossein Barezban, Hamed Mirzadeh, Reza Roumina, Reza Mahmudi, Constitutive analysis of wrought Mg-Gd magnesium alloys during hot compression at elevated temperatures, Journal of Alloys and Compounds, Volume 791, 2019, Pages 1200-1206, ISSN 0925-8388,
10. Ming-Song Chen, Wu-Quan Yuan, Hong-Bin Li, Zong-Huai Zou, New insights on the relationship between flow stress softening and dynamic recrystallization behavior of magnesium alloy AZ31B, Materials Characterization, Volume 147, 2019, Pages 173-183, ISSN 1044-5803, https://doi.org/10.1016/j.matchar.2018.10.031.
11. Rajeshwar R. Eleti, Tilak Bhattacharjee, Akinobu Shibata, Nobuhiro Tsuji, Unique deformation behavior and microstructure evolution in high temperature processing of HfNbTaTiZr refractory high entropy alloy, Acta Materialia, Volume 171, 2019, Pages 132-145, ISSN 1359-6454, https://doi.org/10.1016/j.actamat.2019.04.018.

12. Wang, J., Shen, Y., Liu, Y., Wang, F., & Jia, N. (2019). Tailoring strength and ductility of a Cr-containing high carbon steel by cold-working and annealing. Materials, 12(24),4136. https://doi.org/10.3390/ma12244136
13. Tkalcec, I., & Mari, D. (2004). Internal friction in martensitic, ferritic and bainitic carbon steel; cold work effects. Materials Science and Engineering: A, 370(1-2), 213-217. https://doi.org/10.1016/j.msea.2003.04.004
14. Arioka, K., Miyamoto, T., Yamada, T., & Aoki, M. (2013). Role of cavity formation in crack initiation of cold-worked carbon steel in high-temperature water. Corrosion, 69(5), 487-496. https://doi.org/10.5006/0821
15. Özbek, O., & Saruhan, H. (2020). The effect of vibration and cutting zone temperature on surface roughness and tool wear in eco-friendly MQL turning of AISI D2. Journal of Materials Research and Technology, 9(3), 2762-2772. https://doi.org/10.1016/j.jmrt.2020.01.010
16. Sathish, T., Arul, K., Subbiah, R., Ravichandran, M., & Mohanavel, V. (2021, September). Optimization on end milling operating parameters for super alloy of Inconel 617 by Taguchi's L27 orthogonal array. In Journal of Physics: Conference Series (Vol. 2027, No. 1, p. 012013). IOP Publishing. 10.1088/1742-6596/2027/1/012013
17. Man-Tai Chen, Ben Young, Material properties and structural behavior of cold-formed steel elliptical hollow section stub columns, Thin-Walled Structures, Volume 134, 2019, Pages 111-126,
18. Dami Yim, Praveen Sathiyamoorthi, Soon-Jik Hong, Hyoung Seop Kim, Fabrication and mechanical properties of TiC reinforced CoCrFeMnNi high-entropy alloy composite by water atomization and spark plasma sintering, Journal of Alloys and Compounds, Volume 781, 2019, Pages 389-396, ISSN 0925-8388, https://doi.org/10.1016/j.jallcom.2018.12.119.
19. Rokilan, M., & Mahendran, M. (2020). Elevated temperature mechanical properties of cold-rolled steel sheets and cold-formed steel sections. Journal of Constructional Steel Research, 167, 105851. https://doi.org/10.1016/j.jcsr.2019.105851
20. Klimova, M. V., Shaysultanov, D. G., Zherebtsov, S. V., & Stepanov, N. D. (2019). Effect of second phase particles on mechanical properties and grain growth in a CoCrFeMnNi high entropy alloy. Materials Science and Engineering: A, 748, 228-235. https://doi.org/10.1016/j.msea.2019.01.112
21. H.J. Kong, C. Xu, C.C. Bu, C. Da, J.H. Luan, Z.B. Jiao, G. Chen, C.T. Liu, Hardening mechanisms and impact toughening of high-strength steel containing low Ni and Cu additions, Acta Materialia, Volume 172, 2019, Pages 150-160, ISSN 1359-6454, https://doi.org/10.1016/j.actamat.2019.04.041.
22. DeCost, B. L., Francis, T., & Holm, E. A. (2017). Exploring the microstructure manifold: image texture representations applied to ultrahigh carbon steel microstructures. Acta Materialia, 133, 30-40. https://doi.org/10.1016/j.actamat.2017.05.014
23. Ramakoteswara Rao Veeravalli, Ramanaiah Nallu, Sarcar Mohammed Moulana Mohiuddin, Mechanical and tribological properties of AA7075–TiC metal matrix composites under heat treated (T6) and cast conditions, Journal of Materials Research and Technology, Volume 5, Issue 4, 2016, Pages 377-383, ISSN 2238-7854, https://doi.org/10.1016/j.jmrt.2016.03.011.
24. Kohne, T., Fahlkrans, J., Stormvinter, A., Maawad, E., Winkelmann, A., Hedström, P., & Borgenstam, A. (2023). Evolution of Martensite Tetragonality in High-Carbon Steels Revealed by In Situ High-Energy X-Ray Diffraction. Metallurgical and Materials Transactions A, 1-18. https://doi.org/10.1007/s11661-022-06948-z
25. Yan, X., Yin, S., Chen, C., Huang, C., Bolot, R., Lupoi, R., ... & Liu, M. (2018). Effect of heat treatment on the phase transformation and mechanical properties of Ti6Al4V

fabricated by selective laser melting. Journal of Alloys and Compounds, 764, 1056-1071. https://doi.org/10.1016/j.jallcom.2018.06.076

26. Fuat Kara, Mustafa Karabatak, Mustafa Ayyıldız, Engin Nas, Effect of machinability, microstructure and hardness of deep cryogenic treatment in hard turning of AISI D2 steel with ceramic cutting, Journal of Materials Research and Technology, Volume 9, Issue 1, 2020, Pages 969-983, ISSN 2238-7854, https://doi.org/10.1016/j.jmrt.2019.11.037.
27. Isil Gurten Inal, Zeki Aktas, Enhancing the performance of activated carbon based scalable supercapacitors by heat treatment, Applied Surface Science, Volume 514, 2020, 145895, ISSN 0169-4332, https://doi.org/10.1016/j.apsusc.2020.145895.
28. Alireza Vahedi Nemani, Mahya Ghaffari, Ali Nasiri, Comparison of microstructural characteristics and mechanical properties of shipbuilding steel plates fabricated by conventional rolling versus wire arc additive manufacturing, Additive Manufacturing, Volume 32, 2020, 101086, ISSN 2214-8604, https://doi.org/10.1016/j.addma.2020.101086.
29. Yuka Kajima, Atsushi Takaichi, Nuttaphon Kittikundecha, Takayuki Nakamoto, Takahiro Kimura, Naoyuki Nomura, Akira Kawasaki, Takao Hanawa, Hidekazu Takahashi, Noriyuki Wakabayashi, Effect of heat-treatment temperature on microstructures and mechanical properties of Co–Cr–Mo alloys fabricated by selective laser melting, Materials Science and Engineering: A, Volume 726, 2018,Pages 21-31, ISSN 0921-5093, https://doi.org/10.1016/j.msea.2018.04.048.
30. Rumana Hossain, Farshid Pahlevani, Veena Sahajwalla, Stability of retained austenite in high carbon steel – Effect of post-tempering heat treatment, Materials Characterization, Volume 149, 2019, Pages 239-247, ISSN 1044-5803, https://doi.org/10.1016/j.matchar.2019.01.034.
31. Lv, Z. Q., Wang, B., Wang, Z. H., Sun, S. H., & Fu, W. T. (2013). Effect of cyclic heat treatments on spheroidizing behavior of cementite in high carbon steel. Materials Science and Engineering: A, 574, 143-148. https://doi.org/10.1016/j.msea.2013.02.059
32. Fonstein, N. (2015). Advanced high strength sheet steels (p. 369). New York, NY, USA:: Springer International Publishing. https://doi.org/10.1007/978-3-319-19165-2
33. ElFaham, M. M., Elthalabawy, W. M., Elzahed, O., Zakaria, M. A., & Abdelhamid, M. (2020). Mechanical hardness estimation of heat-treated DIN50Cr3 spring steel utilizing laser-induced breakdown spectroscopy (LIBS) inverse calibration. Applied Physics A, 126, 1-9. https://doi.org/10.1007/s00339-020-3348-4
34. Kosturek, R., Wachowski, M., Śnieżek, L., & Gloc, M. (2019). The influence of the post-weld heat treatment on the microstructure of Inconel 625/carbon steel bimetal joint obtained by explosive welding. Metals, 9(2), 246. https://doi.org/10.3390/met9020246
35. Sivam, S. P., Loganathan, G. B., Umasekar, V. G., Suresh Kumar, P. S., & Raja, S. (2019). Study on Microstructural Characteristics and Mechanical Behaviour of AISI1050 Steel under Various Heat Treatments. International Journal of Vehicle Structures & Systems (IJVSS), 11(1).
36. Adnan, M. A., Kee, K. E., Raja, P. B., Ismail, M. C., & Kakooei, S. (2018, May). Influence of heat treatment on the corrosion of carbon steel in environment containing carbon dioxide and acetic acid. In IOP Conference Series: Materials Science and Engineering (Vol. 370, No. 1, p. 012039). IOP Publishing. 10.1088/1757-899X/370/1/012039
37. Rajendran, T. P., Hynes, N. R. J., Nikolova, M. P., Christopher, T., & Nikolov, D. (2020). Influence of heat treatment on friction-welded joints made of high-carbon high-chromium tool steel/low-carbon steel for tooling applications. Journal of the Brazilian Society of Mechanical Sciences and Engineering, 42(2), 87. https://doi.org/10.1007/s40430-019-2165-1

38. Sebayang, M. D., Yudo, S. M., & Silitonga, C. (2018, March). Effect of heat treatment On Microstructure of steel AISI 01 Tools. In IOP Conference Series: Materials Science and Engineering (Vol. 343, No. 1, p. 012005). IOP Publishing.
39. Gebril, M. A., Aldlemey, M. S., & Kablan, A. F. (2014). Effect of austenization temperatures and times on hardness, microstructure and corrosion rate of high carbon steel. Design and Computation of Modern Engineering Materials, 421-428. https://doi.org/10.1007/978-3-319-07383-5_30
40. Cao, J., Gu, Q., Gao, N., Chen, F., Cheng, C., Wang, Y., & Ma, H. (2021). Designing micro-nano structure of anodized iron oxide films by metallographic adjustment on T8 steel. Ceramics International, 47(23), 32954-32962. https://doi.org/10.1016/j.ceramint.2021.08.194
41. Brian L. DeCost, Toby Francis, Elizabeth A. Holm, Exploring the microstructure manifold: Image texture representations applied to ultrahigh carbon steel microstructures, Acta Materialia, Volume 133, 2017, Pages 30-40, ISSN 1359-6454, https://doi.org/10.1016/j.actamat.2017.05.014.
42. Myoung-Gyu Lee, Sung-Joon Kim, Heung Nam Han, Woo Chang Jeong, Application of hot press forming process to manufacture an automotive part and its finite element analysis considering phase transformation plasticity, International Journal of Mechanical Sciences, Volume 51, Issues 11–12, 2009, Pages 888-898, ISSN 0020-7403, https://doi.org/10.1016/j.ijmecsci.2009.09.030.
43. M. Shirazi, H., Georges, R., Hernandez, R., & Blais, C. (2022). Effect of the cross-rolling and austempering heat treatment on the microstructure, texture, and mechanical properties of a low alloyed steel used in rotary cutting tools. The International Journal of Advanced Manufacturing Technology, 120(5-6), 3787-3804. https://doi.org/10.1007/s00170-022-08911-z
44. T. Sourmail, F.G. Caballero, F. Moudian, D. De Castro, M. Benito, High hardness and retained austenite stability in Si-bearing hypereutectoid steel through new heat treatment design principles, Materials & Design, Volume 142, 2018, Pages 279-287, ISSN 0264-1275, https://doi.org/10.1016/j.matdes.2018.01.035.
45. Behzad Avishan, Majid Tavakolian, Sasan Yazdani, Two-step austempering of high performance steel with nanoscale microstructure, Materials Science and Engineering: A, Volume 693, 2017, Pages 178-185, ISSN 0921-5093, https://doi.org/10.1016/j.msea.2017.03.104.
46. Masoud Sabzi, Saeid Mersagh Dezfuli, Post weld heat treatment of hypereutectoid hadfield steel: Characterization and control of microstructure, phase equilibrium, mechanical properties and fracture mode of welding joint, Journal of Manufacturing Processes, Volume 34, Part A, 2018, Pages 313-328, ISSN 1526-6125, https://doi.org/10.1016/j.jmapro.2018.06.009.
47. Ozioko E. Raphael, Egwuagu M. Onyekachi, Nwankwojike B. Nduka Simulation of Austenitising Temperature and Quench Time for Application Specific based Austempering of Carbon Steels in B-PKO Medium International Journal of Advanced Research in Science, Engineering and Technology Vol. 8, Issue 9 , September 2021 ISSN: 2350-0328
48. Dongyun Sun, Hanqing Zhao, Leilei You, Xiaoyan Long, Zhinan Yang, Yanguo Li, Feng Liu, Fucheng Zhang, Effects of first-step controlling on ultra-fine bainitic steel produced by two-step austempering process, Materials Science and Engineering: A, Volume 845, 2022, 143212, ISSN 0921-5093, https://doi.org/10.1016/j.msea.2022.143212.
49. Skołek, E., Szwejkowska, K., Chmielarz, K., Świątnicki, W. A., Myszka, D., & Wieczorek, A. N. (2022). The Microstructure of Cast Steel Subjected to Austempering and BQ &P Heat Treatment. Metallurgical and Materials Transactions A, 53(7), 2544-2560. https://doi.org/10.1007/s11661-022-06685-3

50. Bernardo, M. A., Ogliare, V., & Domingos, D. (2022). Correlation between Microstructure and Impact Toughness of Austempered High Carbon Steels in Bru State, Silicon, Nickel and Manganese Variant. Journal of Metastable and Nanocrystalline Materials, 34, 19-36
51. Pillai, N., & Karthikeyan, R. (2018, April). Prediction of ttt curves of cold working tool steels using support vector machine model. In IOP Conference Series: Materials Science and Engineering (Vol. 346, No. 1, p. 012067). IOP Publishing. https://doi.org/10.1088/1757-899X/346/1/012067
52. Lv, Z. Q., Wang, B., Wang, Z. H., Sun, S. H., & Fu, W. T. (2013). Effect of cyclic heat treatments on spheroidizing behavior of cementite in high carbon steel. Materials Science and Engineering: A, 574, 143-148.
53. Zambrano, O. A., Valdés, J., Aguilar, Y., Coronado, J. J., Rodríguez, S. A., & Logé, R. E. (2017). Hot deformation of a Fe-Mn-Al-C steel susceptible of κ-carbide precipitation. Materials Science and Engineering: A, 689, 269-285. https://doi.org/10.1016/j.msea.2017.02.060
54. Prusty, B. G., & Banerjee, A. (2020). Structure–property correlation and constitutive description of structural steels during hot working and strain rate deformation. Materials, 13(3), 556. https://doi.org/10.3390/ma13030556
55. Petković, R. A., Luton, M. J., & Jonas, J. J. (1975). Recovery and recrystallization of carbon steel between intervals of hot working. Canadian metallurgical quarterly, 14(2), 137-145. https://doi.org/10.1179/000844375795050201
56. Chandramouli, R., Pandey, K. S., Kandavel, T. K., Ashokkumar, T., & Shanmugasundaram, D. (2007). Influence of material flow constraints during cold forming on the deformation and densification behaviour of hypoeutectoid P/M steel ring preforms. The International Journal of Advanced Manufacturing Technology, 31(9-10), 926-932. https://doi.org/10.1007/s00170-005-0272-x
57. Okonkwo, P. C., Kelly, G., Rolfe, B. F., & Pereira, M. P. (2016). The effect of sliding speed on the wear of steel–tool steel pairs. Tribology International, 97, 218-227. https://doi.org/10.1016/j.triboint.2016.01.030
58. Hentschel, O., Scheitler, C., Fedorov, A., Junker, D., Gorunov, A., Haimerl, A., ... & Schmidt, M. (2017). Experimental investigations of processing the high carbon cold-work tool steel 1.2358 by laser metal deposition for the additive manufacturing of cold forging tools. Journal of Laser Applications, 29(2), 022307.
59. Ezatpour, H. R., Sajjadi, S. A., & Haddad-Sabzevar, M. (2010). Influence of hot deformation strain rate on the mechanical properties and microstructure of K310 cold work tool steel. Materials Science and Engineering: A, 527(6), 1299-1305.
60. Kumar, S., Maity, S. R., & Patnaik, L. (2021). A comparative study on wear behaviors of hot work and cold work tool steel with same hardness under dry sliding tribological test. Materials Today: Proceedings, 44, 949-954.